

Reactor Design for Continuous Monoclonal Antibody Precipitation Based Upon Micro-mixing

Michael Martinez¹, Gareth Mannall¹, Mari Spitali², Edith L Norrant³, Daniel G Bracewell¹

¹Department of Biochemical Engineering, University College London, London WC1E 6BT, United Kingdom

²UCB Pharma, Slough, Berkshire, SL1 4BG, United Kingdom

³UCB Pharma, Braine-l'Alleud, Brussels, Belgium

Correspondence: d.bracewell@ucl.ac.uk (D. G. Bracewell)

ORCID: <https://orcid.org/0000-0003-3866-3304>

Abstract

BACKGROUND: Precipitation has seen application for the processing of important therapeutics including monoclonal antibodies (mAbs). The scale-up proves to be a challenging task due to the complexity of the reactions and transport processes involved. This requires a good understanding of the molecular processes underpinning precipitate formation.

The aim of the study was to build a micro-mixing model for the precipitation of a mAb in continuous tubular reactors using ammonium sulphate. The effect of micro-mixing on precipitate formation with respect to size, strength and nature was evaluated. An ultra scale-down (USD) centrifugation methodology was applied to determine the ease of precipitate clarification.

This article has been accepted for publication and undergone full peer review but has not been through the copyediting, typesetting, pagination and proofreading process which may lead to differences between this version and the [Version of Record](#). Please cite this article as doi: [10.1002/jctb.6652](https://doi.org/10.1002/jctb.6652)

RESULTS: The results demonstrated that the final mean particle size decreased with increased micro-mixing, and was obtained with short residence times. Antibody yields in the tubular reactors were consistently above 90% and shown to be independent of the mixing. Similar particle sizes between a lab and pilot-scale reactor were correlated with the average energy dissipation rate. The smaller particles obtained from improved micro-mixing had higher fractal dimensions which correlated with minimal breakage upon exposure to turbulent shear. Precipitates were easily clarified at the USD scale (> 95% clarification) but less so at pilot-scale (< 80 % clarification).

CONCLUSION: The precipitation is a rapid process with final precipitate properties controlled by the flow conditions. Therefore, the process can be controlled to acquire a certain particle size range. A high-throughput precipitation process is also possible. Further investigation into large-scale precipitate recovery is required.

Keywords: ammonium sulphate precipitation, continuous processing, micro-mixing, ultra scale-down centrifugation, mAbs

Introduction

The complexity of precipitation processes makes it difficult to define the physical and chemical parameters which influence the quality of the precipitate product. Traditionally employed for low-value products, there is now an increased emphasis to develop precipitation processes for high-value products.¹⁻³ Developing a scalable precipitation process for bio-therapeutic manufacture is challenging due to the lack of understanding of the fundamental mechanisms and processes involved. A typical approach to the scale up of a precipitation process is by means of maintaining geometric, dynamic and kinematic parallels between scales. The dimensionless groups including Reynolds number, Damköhler number, Peclet number and Camp Number have all been proposed as suitable scale-up criteria.⁴⁻⁶ Scale-up becomes feasible when all the dimensionless groups controlling the process are maintained at the same value between different scales. In most cases however, this cannot be established and scale-up becomes an empirical process. Reports which successfully demonstrate the scale-up of precipitation processes are rather sparse in the literature.⁷⁻⁹

Precipitation occurs in two phases: nucleation and growth.¹⁰ In the nucleation phase, sub-micron particles are formed. Next, particles grow by colliding with each other via Brownian motion up to a limiting size, after which further growth is governed by the fluid motion and shear field. Both processes occur almost simultaneously at different rates relative to the supersaturation level. The rate of nucleation increases exponentially with supersaturation, whilst the growth rate increases linearly.^{11,12} The objective in producing a protein precipitate is to form large aggregates through the control of the particle growth process, and thus facilitating separation. The rate of nucleation, due to high supersaturation, should be kept to a minimum to avoid the formation of many small particles that become difficult to recover. This can be controlled through efficient mixing regimes that reduce supersaturation gradients. In addition, the formation of aggregates that are resistant to shear disruption is necessary to minimise the breakage of large aggregates into finer particles during industrial

Accepted Article

processing, and so cause minimal impact on the separation efficiency. The precipitate aging process is known to be important in the improvement of particle strength and also density.¹³ The resistance to shear break up has been shown to correlate with the dimensionless Camp number, N_{Ca} , which describes the shear history of precipitate particles and is given by $N_{Ca} = Gt$, where G is the average shear rate and t , the time of exposure to shear. It has been suggested that precipitates with Camp numbers above 10^5 are sufficiently strong to withstand turbulent shear forces.¹⁴ This correlation has been identified in the aging of soya precipitate via isoelectric precipitation.¹⁵

The influence of mixing on the physical properties of chemical and biological-based precipitates has been studied vigorously.^{16–18} Based on the studies, scale-up on the basis of mixing using the specific power input and tip speed constants have been proposed for batch precipitations. The challenge arises when more than one mixing mechanism (e.g. micro-mixing, meso-mixing and macro-mixing) is controlling the process, and thus the final product is affected due to the variation of flow patterns between scales. Therefore, using a constant tip speed or constant specific energy input could lead to unsatisfactory large-scale predictions. Some authors have shown that when the mixing mechanism is limited to micro-mixing, constant power per unit volume provides good scale-up predictions.^{9,19} In order to ensure a micro-mixing controlled process in a batch reactor, the rate of feeding has to be an order of magnitude slower than the circulation rate governed by macro-mixing. This often requires slow feeding rates and reduces process throughput.

Continuous reactors, such as tubular reactors, offer a promising approach to precipitation unit operations as these can achieve higher throughputs.^{20–23} Moreover, these systems can achieve superior mixing times based on the specific design elements, including mixer selection and bore size. This is particularly important for fast precipitation reactions where the nucleation and growth processes occur spontaneously. Since nucleation and growth are molecular level processes, micro-mixing becomes relevant in describing the transport mechanisms involved. When the reaction time of the process is shorter than the mixing time,

the process is controlled by the intrinsic kinetics without the influence of micro-mixing. Conversely, when the mixing time is shorter or on the same magnitude as the reaction time, the reaction is influenced by micro-mixing. In the case where inefficient micro-mixing yields precipitate particles with undesired properties, then a reactor design should focus on achieving complete micro-mixing before the onset of the precipitation reaction.

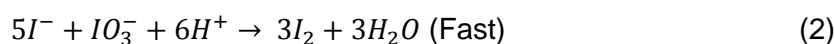
Despite the abundance of studies concerning micro-mixing phenomena in continuous reactors, few discuss the potential for scale-up and even its application for a large-scale precipitation process. One scale-up approach has however been established for the precipitation of Lovastatin using a two-impinging jets (TIJ) precipitator based on micro-mixing.⁴ The study demonstrated how the magnitude of the micro-mixing time to the nucleation time controlled the particle size distribution (PSD) of Lovastatin precipitates. Thus, the Damköhler constant was proposed for scale-up. Moreover, they concluded that the TIJ precipitator was capable of achieving very short micro-mixing times for the generation of a homogeneously supersaturated solution prior to the nucleation time. This study amongst others come to a general agreement that localised supersaturation gradients influenced by mixing is the key factor in controlling particle size and PSD by influencing nucleation and growth rates.

In this work, the influence of micro-mixing in T-mixer continuous tubular reactors on the salt precipitation of an immunoglobulin from mammalian cell culture supernatant was examined. At the same time, micro-mixing was evaluated as a tool for scale-up. In addition, we studied the link between final precipitate properties (e.g. particle size, PSD, morphology and fractal dimension) and ease of separation by centrifugal recovery using an ultra-scale down centrifugation (USD) methodology. Finally, the USD clarification results were verified with a disc-stack centrifugation run.

Theoretical considerations

Micro-mixing

Chemical models to evaluate micro-mixing quality in various reactor designs have been under much development. For instance, the iodide-iodate and diazo coupling between naphthol and diazotized sulphanilic acid methods are frequently used for micro-mixing tests in stirred and in-line mixing reactors.^{24,25} These rely on the selectivity of competitive reactions which directly correlate to the micro-mixing efficiency. In particular, the iodide-iodate micro-mixing test developed by Villermaux²⁶ is simple and adaptable in examining viscous effects on mixing quality. Therefore, the iodide-iodate reaction test was proposed to evaluate micro-mixing. The reaction scheme comprises the following three reactions:



Reactions (1) and (2) both consume and compete for acid at different rates. Reaction (1) is instantaneous, while Reaction (2) is fast, but slower than Reaction (1) and is comparable to the micro-mixing process. The rate of Reaction 2 is given by:

$$r = k[H^+]^2[I^-]^2[IO_3^-] \quad (4)$$

where k is a function of the ionic strength, I , of the mixture:

$$\text{If } I < 0.16 \text{ M then: } \log(k) = 9.28 - 3.66\sqrt{I} \quad (5)$$

$$\text{If } I > 0.16 \text{ M then: } \log(k) = 8.38 - 1.5115\sqrt{I} + 0.23I \quad (6)$$

In the presence of acid, as long as the pH is kept above 9 upon good mixing, Reaction (2) does not occur to a significant extent in relation to Reaction (1). However, when local

excesses of acid occur as a result of inefficient mixing, Reaction (2) proceeds and I_2 formation occurs. I_2 then becomes instantly trapped by I^- to form I_3^- in Reaction (3). The equilibrium constant, K_B , for Reaction (3) is a function of the temperature T:

$$\log(K_B) = \frac{555}{T} + 7.355 - 2.575 \log T \quad (7)$$

The amount of I_3^- produced allows the characterisation of the micro-mixing efficiency through the segregation index X_s . The segregation index X_s is defined as Y/Y_{ST} where Y is the ratio of acid mole number consumed by Reaction (2) to the total acid mole number injected ($Y = 2(n_{I_2} + n_{I^-})/n_{H^+}$) and Y_{ST} is the value of Y in the case of total segregation when the micro-mixing process is infinitely slow ($Y_{ST} = 6[IO_3^-]_0 / (6[IO_3^-]_0 + [H_2BO_3^-]_0)$). The value of X_s is within the range $0 < X_s < 1$ for partial segregation. For $X_s = 0$, perfect micro-mixing is indicated, whereas total segregation is indicated for $X_s = 1$. The amount of I_2 can be determined based on a mass balance of iodine atoms and the value of K_B .

Fractal dimension

A particle in three-dimensional space is considered to be fractal if its density decreases with radial distance from the nucleus. An assessment of the fractal geometry of particles may provide a useful insight into the characterisation of protein precipitates which influence their behaviour during solid-liquid separation. Fractal dimension analyses were first described as a method of elucidating the process of diffusion-limited colloidal aggregation, upon which lead to the formation of clusters with particular structures.²⁷ The fractal dimension, f_D , has a value less than 3 and is a non-integer. In the case of a straight line, f_D is 1; for a circle in two-dimensional space, f_D is 2, and for a perfectly spherical aggregate which is uniformly packed of primary particles; f_D is 3. For the typical branched and porous nature of particle structures

often obtained from aggregation and/or precipitation processes, f_D will have a value less than 3.

In addition to acquiring PSD data from laser light scattering methods, it is also possible to extract scattering angle and light intensity data information which provides estimations of f_D . In the Malvern Mastersizer 3000, which has a particle size detector range of 0.1 to 1000 μm , 68 detectors are placed at unique scattering angles that detect particles within a particular size range. The scattering wave vector, Q , is a function of the scattering angle, Θ , and corresponds to the inverse of a particular particle radius which is given by:

$$Q = \frac{4\pi n_i}{\lambda} \sin\left(\frac{\Theta}{2}\right) \quad (8)$$

The scattering pattern of deflected laser light with intensity, I , at each Θ is a function of the number of aggregate particles at the corresponding particle size, and is characteristic of the nature of the particle structures. The number of particles present within the aggregate is a function of f_D and I which is expressed as:

$$\text{Log}I = k - f_D \text{Log}Q \quad (9)$$

where k is a proportionality constant. Plotting $\text{Log}Q$ against $\text{Log}I$ gives a negative slope by which the fractal dimension is estimated.

Experimental

Materials

Clarified Chinese hamster ovary (CHO) cell culture supernatant (serum free) secreting monoclonal immunoglobulin G4 antibody (IgG₄) with a titer of 1.5 mg/mL was harvested at UCB Pharma (Slough, UK). The CCCF material provided is a research candidate and therefore not dedicated for a therapeutic process. Clarification was accomplished by a

Accepted Article

combination of centrifugation and depth filtration. The supernatant was stored at – 20°C (long term) or 4°C (short term). Increasing antibody titer in the supernatant was performed by spiking the supernatant with antibody solution, pre-purified by Protein A and concentrated to 50 mg/mL by ultra-/dia-filtration using a 30 kDa molecular weight cut off (MWCO) membrane (T-series cassette, Pall Life Sciences).

Monosodium phosphate monobasic, disodium phosphate dibasic and ammonium sulphate were purchased from Sigma Aldrich. Glycine, hydrochloric acid and sodium hydroxide were purchased from Fisher Scientific. Buffer and stock solutions were degassed and filtered through 0.22 µm membranes.

Methods

Ammonium sulphate precipitation

The ammonium sulphate precipitation was performed in two self-constructed tubular reactors: one at lab-scale (Figure 1A) and one at pilot-scale (Figure 1B). The lab-scale reactor was equipped with a micro-T mixer (Upchurch Scientific, UK) with an internal diameter of 0.5 mm. Tubing of 0.5, 1 and 2 mm internal diameter was connected to the T outlet. A small length of 1 mm diameter tubing (approximately 5 cm) was inserted between the T outlet and 2 mm diameter tubing to allow connection. The reactor tubing length was varied between 1 and 10 m to determine the required residence time to complete the precipitation. Pumping of solutions was accomplished with a Harvard Apparatus PHD ULTRA double-barrelled syringe pump (Harvard Apparatus, UK) fitted with either 20 or 50 mL Plastipak syringes.

The pilot-scale reactor was equipped with a T-mixer (Swagelok, UK) with an internal diameter of 4.8 mm. At the outlet, tubing of 6.4 mm diameter and 5 m in length was arranged in the form of a coiled-flow inverter reactor (CFIR) similar to ²⁸. The arrangement consisted

of eight helical turns around a PVC pipe with a diameter of 75 mm, followed by a 90° bend, and finally eight additional helical turns. The main and gradient pumps of an AKTA Ready system (GE Healthcare, UK) were used to feed solutions through the reactor. In each reactor, 3 M ammonium sulphate was dosed to 1.5 M in a single step at the T mixer entrance. All precipitations were performed at pH 7 and at ambient temperature. Five space times were allowed before collecting precipitate samples at the reactor exit for analysis. Lab-scale experiments were carried out in triplicate, whilst pilot-scale experiments were carried out in duplicate.

Protein A affinity chromatography

Mabselect Sure resin (GE Healthcare, Uppsala, Sweden) was packed in a XK50 chromatographic column according to the manufacturer's instructions. The resin bed height was 20 cm. The column was equilibrated with 5 columns volumes (CV) of equilibration buffer (Dulbecco's PBS, pH 7.4), then the CHO supernatant was loaded onto the column at 150 cm/h. Column washing was then performed with equilibration buffer for 5 CV. 100 mM sodium citrate pH 3.6 was used as the elution buffer. CIP was performed with 0.5 M NaOH.

Micro-mixing experiments

A glycerol-water solution (21% v/v) was used to mimic the ammonium sulphate solution viscosity. Glycerol mixtures have been reported by Guichardon *et al.*²⁹ to investigate micro-mixing in viscous systems. In our experiments, boric acid solution was added to sodium hydroxide to obtain a mixture buffer solution. Potassium iodide and potassium iodate solutions were then added in sequence, to which the mixture was supplemented with water and glycerol to target reagent concentrations. The final mixture was comprised of the following reagent concentrations: 0.045 M boric acid, 0.003 M potassium iodate, 0.016 M

Accepted Article

potassium iodide and 21 % v/v glycerol. The sulfuric acid concentration was 0.015 M, corresponding to 0.03 M H⁺. Buffer and sulfuric acid solutions were fed into the continuous reactors at equal flow rates. The amount of tri-iodide produced at the reactor outlet was determined by a spectrophotometer at 353 nm. All experiments were conducted at ambient temperature with recordings of the effluent being in the range 22.5 to 23.5°C. The micro-mixing tests were performed in triplicate. The variance in X_s was less than ± 5 %

Particle Size Distribution

Precipitate samples were evaluated using blue and red (laser) light diffraction through a sample flow cell (Mastersizer 3000, Hydro SV dispersion unit, Malvern Instruments Ltd., Worcestershire, UK) working in the particle size detection range 0.1 – 1000 μm . In the sample flow cell, samples were dispersed with 1.5 M ammonium sulphate pH 7, reaching a target laser obscuration in the range 10 – 20 %. Five individual measurements were taken and then recorded as volume percentage. Representative size distributions are presented from triplicate preparations from the lab-scale experiments and duplicate preparations from the pilot-scale experiments. The relative standard deviation of size distributions was less than $\pm 10\%$.

Microscopy

Processed samples were loaded onto pre-cleaned glass microscopic slides (VWR, UK) with cover slips (VWR, UK). Phase contrast images were taken with a Nikon TE2000-PFS inverted microscope (Nikon, UK) and processed with Image J.

Disc-Stack Centrifugation

A pilot-scale clarification run was performed using the GEA Westfalia Pathfinder PSC 1-06-177 (GEA Westfalia, Germany) at 13,500 rpm (20,000 × g) with a flow rate of 35 L/H. PSC-1 has 8 discs, a bowl volume of 1 L and a solids capacity of approximately 850 g. Pre-operation set-up was performed according to the manufacturer's instructions. The centrifuge bowl and equipment piping were filled with reverse osmosis water to test the efficiency of bowl opening and closing. During constant agitation, feed was pumped through the centrifuge via a centripetal pump for a total of 7 minutes. The supernatant was collected after 1 min of processing. A precipitate wash step was performed by feeding ~ 4 L of 1.5 M ammonium sulphate through the system. The captured solids were discharged from the bowl by three complete discharges. Samples taken forward for analysis included feed, centrate and the discharged solids.

Ultra Scale-Down Centrifugation Studies

Precipitate samples were exposed to turbulent shear stress for 20 s in a rotary disc device. The construction of the device is detailed elsewhere.³⁰ 20 mL of sample was exposed to 6000 rpm shear, as equivalent to the condition experienced in the feed zone of a hydro-hermetic disc stack centrifuge. This corresponded to a maximum energy dissipation rate of $0.045 \times 10^6 \text{ Wkg}^{-1}$.³¹ Each shear preparation was carried out in duplicate and tested for sedimentation in a lab-scale centrifuge. Non-sheared samples were also tested for sedimentation as a reference. Sedimentation properties were characterized in terms of equivalent settling area (Σ_T):

$$\Sigma_T = \frac{V_{lab}\omega^2}{2g \ln\left(\frac{2R_o}{R_o+R_i}\right)} \quad (9)$$

where V_{lab} is the volume of feed processed in the centrifuge tube, ω is the angular velocity, g is the acceleration due to gravity, R_i is the inner radius (the distance between the centre of rotation and the top of the liquid) and R_o is the outer radius (the distance between the center of rotation and the bottom of the tube). Centrifuge tubes were filled with sample volumes of 1, 1.5 or 2 mL and spun at speeds of 4000 or 8000 rpm for 10 min. The top 50 % of the resulting supernatant was recovered with minimal disturbance of the solids sediment. Well-clarified supernatant was obtained by centrifuging at 16000 x g for 30 min as a baseline for clarification. Clarification was recorded in terms of the solids content, estimated by OD at 600 nm. The percentage of solids remaining, S, was characterised by:

$$S (\%) = 100 \times \frac{OD_S - OD_o}{OD_F - OD_o}$$

where OD_s is the optical density of the supernatant, OD_F is the optical density of the feed prior to centrifugation and OD_o is the optical density of the well-spun sample.

Determination of IgG₄ concentration

The IgG concentration in all samples was determined by analytical protein G affinity chromatography. A 1 mL HiTrap Protein G column was connected to an Agilent 1200 HPLC system (Agilent, UK). 20 mM sodium phosphate pH 7 and 20 mM glycine pH 2.8 were used as the equilibration/wash and elution buffer, respectively. 100 uL injections of samples were made. The flow rate through the system and column was 1 ml/min. The unknown antibody concentration was calculated from a calibration curve prepared from a similar IgG₄ molecule.

Results and Discussion

Determination of Micro-mixing Time

Micro-mixing times in continuous flow systems are estimated using micro-mixing models. The incorporation model proposed by Fournier *et al.*²⁶ has originally been applied to estimate micro-mixing times in turbulent flow, but is equally applicable in laminar flow systems.³² The model assumes that the incoming acid is divided into aggregates and is progressively invaded by the fluid containing the borate-iodate-iodide buffer mixture. The acid aggregates grow progressively incorporating the surrounding liquid where the reactions take place. The characteristic time of incorporation, t_m , is assumed to be equivalent to the micro-mixing time. The aggregate volume grows according to the equation $V_2 = V_{20}g(t)$, where $g(t)$ is the incorporation function and is given by $g(t) = \exp(t/t_m)$. The concentrations of j species, according to the model, are given by:

$$\frac{dC_j}{dt} = \frac{C_{j10} - C_j}{t_m} + R_j$$

where C_j denotes the concentration of reactants in the system, C_{j10} represents the initial concentration of reactants in the surrounding liquid and R_j is the net production rate of each reactant. By assuming a series of t_m values, the concentration of species can be calculated by solving the differential equations for each of the species. Details of the method are presented elsewhere.³³ Upon determining the concentrations of I_2 and I_3^- based on the initial experimental conditions, X_s can be derived.

The theoretical relationship between t_m and X_s as calculated from the incorporation model based on the reagent concentrations selected for the micro-mixing test is shown (Supporting information, Figure S1). The region of t_m range is highlighted according to the experimental

Accepted Article

values of X_s , and thus was used to relate the various process conditions to a characteristic t_m value. The micro-mixing times achieved in the continuous reactors as a function of Reynolds number is displayed in Figure 2. It can be seen that for both reactors, an increase in Reynolds number improved the micro-mixing due to the increased turbulence. In the lab-scale reactor, for a given Re, t_m was in the range 0.001 to 0.012 s (Figure 2A). At the same Re, improved micro-mixing times were observed in the 0.5 mm diameter tubing over the 1 mm and 2 mm diameter tubing. This is due to the improvement of the rate of diffusion by reducing the length of molecular diffusion between lamellae in a smaller tube size. This finding is consistent from previous observations made by Gobert *et al.*³⁴ The similar micro-mixing times between the 1 and 2 mm diameter tubes at the same values of Re could be attributed to the insertion of the short 1 mm diameter tubing between the T outlet and downstream 2 mm diameter tubing. It is suggested that most of the mixing had occurred in this short section and thus improved the overall mixing efficiency. In support of this, Panić *et al* have demonstrated that short capillary lengths are sufficient in completing micro-mixing.³⁵ In the pilot-scale reactor, t_m was in the range 0.0005 to 0.0035 s (Figure 2). The combination of increased turbulence and better radial mixing owing to the helical coiling of the tubing improved micro-mixing times, particularly at higher Re where flow is turbulent. As expected, the determined micro-mixing in the continuous reactors was superior to those reported in conventional stirred-batch reactors.³⁶

Effect of flow rate and residence time on particle size, PSD and yield

The reactor length required to complete the precipitation was determined in the lab-scale reactor using 1 mm diameter tubing. Precipitations were first carried out using a length of 10 m which followed reduction to 5, 4, 3, 2 and 1 m. The flow rate through the system was manually adjusted to 1, 2, 4, 10, 14 or 20 ml/min. Precipitation was assumed to be complete when the mean particle size was at a stable value.

The evolution of mean particle size at the various flow rates over the reactor lengths are displayed in Figure 3. It can be seen that for 1, 2 and 4 ml/min, the initial mean particle size changed over a few meters of tubing up to 5 m. Thereafter, the same particle size was obtained at 10 m. To ensure the precipitation was complete, the reactor effluent for each of the conditions was collected in a batch reactor and continuously stirred, at 300 rpm with a mechanical stirrer, for up to an hour. No further change in particle size was observed indicating precipitation was already completed in the continuous reactor. At the higher flow rates, the initial particle sizes did not appear to change during the course of the process. This suggested that the final equilibrium particle size was obtained very quickly at fast micro-mixing times. Moreover, the mean particle size decreased as the flow rate increased. This could be explained through enhanced mixing which increases the shear exposure on the precipitates, and in turn induce particle breakage events.

Figure 4 displays representative micrographs of the precipitates obtained at 1, 2, 4, 7 and 14 ml/min. In the case of the 20 ml/min condition, a similar result to the 14 ml/min condition was obtained. The micrographs show that precipitates form aggregates of primary particles with amorphous structures. Particles occasionally agglomerated during microscopic analysis which was likely due to the stacking of smaller particles in undiluted samples, thereby appearing as larger aggregates than those determined from laser diffraction. Therefore, laser diffraction was primarily relied on to determine particle sizes, whilst microscopy was useful in informing gross structural differences between particle samples. Nonetheless, the images showed an increased abundance of smaller particles at the higher flow rates. The shift of the mono-modal PSDs with increasing flow rate, confirmed the predominance of a micro-mixing regime controlling the precipitation reaction (Supporting information, Figure S2).

Precipitates obtained after processing through 5 and 10 m of tubing were recovered by centrifugation and re-solubilised up to half the original volume with 50 mM sodium phosphate

buffer. Depending on the flow rate, antibody yields were in the range 91.3 to 94.6%. This indicated that the operating flow rate did not have a clear effect on the yield. Since no change in the yield and particle size result was observed after 5 m of processing, future precipitation experiments were performed at this length.

Effect of protein concentration on particle size

The effect of antibody concentration in the CHO supernatant using the same conditions and reactor system employed above was evaluated. It can be generally seen from Figure 5 that larger mean particle sizes were obtained as the concentration of antibody in the CCCF increased. This effect however becomes negligible at higher flow rates. As the protein concentration in the sample increases, so does the number of particles that precipitate out of solution. Consequently, the particle collision frequency is enhanced to the second power due to the reduction of the diffusional distance barriers between primary particles¹³ (assuming a collision is governed by two particles and results in their adhesion with a 100% success rate). At low mass flow rates, these collisions lead to incremental particle adhesion which ultimately forms larger aggregates under the low shear environments. Conversely, the minimal effect of protein concentration on particle size at high flow rates suggested a hydrodynamic force exposure limitation was imposed on particle growth as a result of forceful impacts between particles. Thus, leading to enhanced particle disruption.

Effect of tube diameter in the lab-scale reactor

Figure 6 displays the precipitate sizes obtained using the 0.5, 1 and 2 mm diameter tubing as a function of Re and energy dissipation rate, ϵ . The same flow rates used during the micro-mixing experiments were employed to demonstrate the relation between micro-mixing times and mean particle size. It can be seen that at a constant Re value for $Re < 110$, larger mean particle sizes were obtained as the tube diameter increased (Figure 6A). When

switching to the 2 mm diameter tubing, precipitate settling in the tube was encountered at < 8 ml/min ($Re < 80$) due to the inefficient force to maintain a homogenous suspension throughout the reactor; thus providing unreliable particle size measurements. Despite the short 1 mm diameter contraction providing better initial mixing at low flow rates, increased flow rates were required to ensure continuous mixing of the precipitate with the mother liquor. Therefore, the flow rate range in these experiments was adjusted to 8 – 85 ml/min. This range may have been more applicable to assess micro-mixing without the 1 mm diameter tubing contraction.

When normalizing the data to energy dissipation rate, it was found that similar particle sizes were obtained between the three tube sizes at similar ϵ (Figure 6B). This suggests that the mechanistic and transport processes involved during precipitate formation to a desired particle size can be controlled with constant ϵ which provides similar micro-mixing behaviour.

Pilot-scale precipitation results

Precipitations in the pilot-scale reactor were performed using flow rates in the range 9 to 150 L/H. The mean particle sizes from duplicate runs are displayed in Figure 7A. Both sets of runs provided comparable results. As in the small-scale, the PSD shifted to smaller and narrower distributions with increasing flow rate (Supporting information, Figure S3). According to Figure 7B, at the lower end of the energy dissipation rate range, the mean particle sizes were smaller than those obtained in the small-scale reactor, but more similar at higher rates. This could be attributed to better micro-mixing times obtained at low energy dissipation rates using the specific reactor design. The micro-mixing times became more similar as the energy dissipation rate increased. Similarly to small-scale, antibody yield was not significantly impacted by the operating flow rate and was in the range 90.9 to 96.1 %.

Effect of turbulent processing

Protein precipitates are known to experience breakage to a certain extent when exposed to the turbulent environments of industrial equipment including pumps and large-scale centrifugation equipment.⁵ A precipitate which undergoes significant breakage reduces the capacity of a disc-stack centrifuge to capture the solids and is therefore carried over into the supernatant, leading to product loss. Hence, a protein precipitate should be sufficiently strong to withstand these forces to optimise separation. Investigating centrifugation conditions at large scale can be costly and reduces the experimental throughput due to the volume of sample required per run. Therefore, the rotating disc device is useful to mimic a vast range of process conditions whilst requiring small sample volumes.

Using a shear rate of 6000 rpm, the change in mean precipitate particle sizes for the various process conditions was evaluated. In addition, the precipitates were characterised in terms of their f_D values as a potential indicator to describe particle strength based on the relative breakage observed. For these experiments, precipitate samples generated from the lab-scale reactor using 1 mm diameter tubing and from the pilot-scale reactor were tested. The results are summarised in Figures 8 and 9. At both scales, there was a clear positive correlation between the applied flow rate and particle breakage upon turbulent shear stress. Larger particles formed at low flow rates, or low mixing, were more susceptible to breakage than the smaller particles formed at high flow rates, or with faster mixing. For example, the maximum percentage size reduction was 60 % for the large precipitates, whilst the smaller precipitates reduced in size by 26 % or less. Moreover, there was a second correlation with the precipitate fractal dimension. Based on studies conducted on whey precipitation by Byrne *et al.*⁸, smaller precipitates possess higher fractal dimensions due to their increased compactness, and are tougher than larger particles with lower fractal dimensions. The results shown here are in agreement with their observations. Although large precipitates are ideal to facilitate separation, the precipitates were weak and fragmented easily with industrial processing, which may in turn reduce centrifugal efficiency.

Ultra Scale-Down Centrifugation

Centrifugation conditions studied for the sedimentation behaviour of non-sheared and sheared samples were selected to represent those equivalent for a disc-stack centrifuge, $(Q/\Sigma) = (V_{lab}/t_{lab}/\Sigma_{lab}) > 3 \times 10^{-9}$ m/s. The comparison of the centrifugal recovery for non-sheared and sheared precipitates formed during lab-scale and pilot-scale continuous processing, as a function of $V_{lab}/\Sigma_{lab}t_{lab}$, i.e. centrifuge throughput, in the range 9.25×10^{-9} to 4.8×10^{-8} m/s, is presented in Figures 10 and 11, respectively. As expected, for a given condition, the percentage of solids remaining was proportional to the centrifuge throughput. Since t_{lab} was a fixed value at 10 min, the larger the value of V_{lab} which influences the settling area, the greater the distance a given solid has to travel and thus settle under centrifugal forces.

For the control samples which were not exposed to shear in the rotating disc device, solids remaining were in the range 0.06 to 0.9% for the lab-scale reactor (Figure 10), whilst for the pilot-scale reactor, the range was 0.01 to 1.2 % (Figure 11). For the sheared samples, solids remaining were in the range 0.4 to 2.7 % and 0.01 to 1.5 % for the lab and pilot-scale reactors, respectively. For a given centrifuge throughput, the clarification of sheared and non-sheared samples were more similar in the pilot-scale reactor than in the lab-scale reactor. The results demonstrate that the clarification of precipitates formed at higher flow rates or with better mixing is less impacted after being exposed to turbulent shear.

Pilot scale centrifugation results

In order to validate the USD centrifugation method in predicting precipitate recovery at pilot scale, a process run on a Pathfinder PSC-1 was performed. Precipitate feed was first prepared in the pilot-scale reactor using a flow rate of 150 L/H which enabled a fast process without affecting protein recovery (93.5 %). Approximately 4 L of feed was processed

through the Pathfinder at a feed flow rate of 35 L/H, which corresponded to a Q/Σ value of 2.52×10^{-8} m/s as selected from the median of the centrifuge throughput tested range.

A useful component of the PSC-1 design is the sight glass incorporated in the feed and supernatant lines which enable monitoring of liquid clarity in real-time, and provide a qualitative indication of centrifugal performance. Also, this allowed monitoring of solids breakthrough as the bowl reaches capacity, at which point the solids discharge mechanism should take place. Initially, a clear supernatant was observed during the first minute of operation. After this, the clarity of the liquid decreased and appeared to be constant for the rest of the run. Visual observation of the supernatant pool showed the presence of precipitate solids which were not effectively clarified. Based on OD_{600} measurements, the solids remaining percentage was 26.2%. This was clearly different to the value predicted from the USD experiments (0.55 ± 0.14 % solids remaining). Replicates would be required to confirm the observation as a real result. It is unlikely that solids breakthrough due to reaching bowl capacity would have occurred since the total amount of solids loaded were approximately 100 g and the capacity of the bowl is about 850g. When the solids present in the supernatant pool were characterised in terms of PSD, a very broad additional peak showing particle sizes in the range 20 -120 μm in relation to the feed material, was observed, as shown in Figure 12A. This could be attributed to the remains of potential air-liquid interfaces formed despite back pressure having been applied on the supernatant discharge. An important factor to consider is the time between sample shearing and clarification. In the USD method, some time passes from the moment of shear exposure in the disc device to the centrifugation step. In a disc-stack centrifuge, the time between particles passing through the feed zone to the settling region is very short. It is possible that during USD characterisation at laboratory scale, that the precipitates undergo a reformation phase shortly after initial breakage. This does not occur in the disc-stack centrifuge because of the very short residence time. Consequently, the phenomenon of hindered settling increased the clarification performance with the USD method. For a more accurate

comparison, precipitates could be diluted for the USD experiments to minimise potential reformation.

The integrity of the precipitate solids upon discharge was assessed and thus indicated the potential of disc-stack centrifugation for separation. For some centrifuges, it is possible to sample the bowl without the need for discharging. This approach allows in understanding the impact of entry into the bowl imposed on the feed particles during operation. This was however not possible for the PSC-1. Instead, we attempted to isolate any solids material which may not have been effectively discharged at the end of the run; however we failed to observe any notable material which could be sampled. The USD experiments consider the shear levels encountered in the feed zone of a disc-stack centrifuge but they do not consider the shear stress field present during solids discharge. It is expected that the shear from discharge is markedly higher than what can be predicted with our USD method. Chan and colleagues previously employed a USD capillary device to study the impact of shear stress on *Escherichia coli* cell breakage during discharge recovery.³⁷ However, the effects on cell recovery were not investigated with pilot-scale centrifugation. Discharge on the precipitate solids was initially thought to induce significant particle fragmentation due to the very high levels of shear. However, as can be seen from Figure 12A, a clear shift in the PSD profile towards larger sizes relative to the feed material with a much broader distribution was observed. The micrographs in Figure 12B and Figure 12C show that the feed particles conglomerated into large structures by a stacking effect. This is likely to be an effect of concentrating the solids within the confined volumes between the bowl discs and/or compacting in the solids collection area. Not to our surprise, the level of solids dewatering was rather poor due to not operating the centrifuge optimally. As a result, approximately half of the soluble phase consisting of many non-precipitated impurities was gathered with the solids. Therefore, further work in optimising a disc-stack centrifuge for this application is needed.

Conclusion

The precipitation of an antibody in clarified cell culture supernatant with ammonium sulphate was a very rapid process controlled by micro-mixing. This makes the unit operation suitable for continuous manufacturing. The tubular precipitator carries the advantage of being a simple and inexpensive design, requiring a small holdup volume to complete the precipitation. Operating at fast flow rates did not impact performance in terms of antibody recovery, indicating that the process can be made high throughput depending on the pump and pressure drop limitations. The extent of micro-mixing during contact between the salt and protein streams depicted the final properties of the precipitate through control of the particle nucleation and growth processes. Control of the final precipitate size can be exerted by regulating the flow conditions in the tubular reactor, which influences the mixing. Enhanced micro-mixing produced smaller particles with narrower PSDs which are additionally tougher than large aggregates and well-clarified with centrifugation. The fractal dimension measurement proved useful as an indicator to describe the nature of precipitates in terms of particle strength and compactness. The difference in clarification performance between the USD methodology and the pilot-scale centrifugation run suggested the need to make adjustments to the USD methodology to account for potential hindered settling to make better predictions. Alternative methods could be more suited for the application and inquire investigation. This could include tubular bowl³⁸ and multi-chamber bowl centrifuges³⁹, as well as various filtration systems including tangential flow filtration^{20,40} and depth filtration.⁴¹

Acknowledgements

This work was supported by the UK Engineering and Physical Sciences Research Council (EPSRC) grant EP/L01520X/1 and UCB Pharma.

References

1. Balasundaram, B., Sachdeva, S. & Bracewell, D. G. Dual salt precipitation for the recovery of a recombinant protein from *Escherichia coli*. *Biotechnol. Prog.* **27**, 1306–1314 (2011).
2. Giese, G., Myrold, A., Gorrell, J. & Persson, J. Purification of antibodies by precipitating impurities using Polyethylene Glycol to enable a two chromatography step process. *J. Chromatogr. B. Analyt. Technol. Biomed. Life Sci.* **938**, 14–21 (2013).
3. Singh, N. *et al.* Clarification technologies for monoclonal antibody manufacturing processes: Current state and future perspectives. *Biotechnol. Bioeng.* **113**, 698–716 (2016).
4. Mahajan, A. J. & Kirwan, D. J. Micromixing effects in a two-impinging-jets precipitator. *AIChE J.* **42**, 1801–1814 (1996).
5. Ayazi Shamlou, P., Stavrinides, S., Titchener-Hooker, N. & Hoare, M. Growth-independent breakage frequency of protein precipitates in turbulently agitated bioreactors. *Chem. Eng. Sci.* **49**, 2647–2656 (1994).
6. Hoare, M. PROTEIN PRECIPITATION AND PRECIPITATE AGING .2. GROWTH OF PROTEIN PRECIPITATES DURING HINDERED SETTLING OR EXPOSURE TO SHEAR. *TI CHEM Eng-I.* **60**, 157–163 (1982).
7. Mahajan, A. J. & Kirwan, D. J. Micromixing effects in a two-impinging-jets precipitator. *AIChE J.* **42**, 1801–1814 (2018).
8. Byrne, E. P., Fitzpatrick, J. J., Pampel, L. W. & Titchener-Hooker, N. J. Influence of shear on particle size and fractal dimension of whey protein precipitates: implications for scale-up and centrifugal clarification efficiency. *Chem. Eng. Sci.* **57**, 3767–3779 (2002).

9. Zauner, R. & Jones, A. G. Scale-up of Continuous and Semibatch Precipitation Processes. *Ind. Eng. Chem. Res.* **39**, 2392–2403 (2000).
10. Nelson, C. D. & Glatz, C. E. Primary particle formation in protein precipitation. *Biotechnol. Bioeng.* (1985). doi:10.1002/bit.260271007
11. Nielsen, A. E. & Belcher, R. *Kinetics of Precipitation*. (Pergamon Press; [distributed in the Western Hemisphere by Macmillan, New York], 1964).
12. Harrison, R. *Protein purification process engineering*. **18**, (1994).
13. Bell, D. J., Hoare, M. & Dunnill, P. The Formation of Protein Precipitates and Their Centrifugal Recovery. in *Advances in biochemical engineering/biotechnology* 1–72 (Springer, 1983).
14. Camp, T. R. *Flocculation and Flocculation Basins*. (American Society of Civil Engineers, 1953).
15. Bell, D. J. & Dunnill, P. Shear disruption of soya protein precipitate particles and the effect of aging in a stirred tank. *Biotechnol. Bioeng.* **24**, 1271–1285 (1982).
16. Iyer, H. & Przybycien, T. Protein precipitation: Effects of mixing on protein solubility. *Am. Inst. Chem. Eng. J.* **40**, 349–360 (1994).
17. Momonaga, M., Yazawa, H. & Kagara, K. Reactive crystallization of methyl ac-methoxyimino acetoacetate. *J. Chem. Eng. Japan* (1992). doi:10.1252/jcej.25.237
18. Salt, D. J., Leslie, R. B., Lillford, P. J. & Dunnill, P. Factors influencing protein structure during acid precipitation: A study of soya proteins. *Eur. J. Appl. Microbiol. Biotechnol.* (1982). doi:10.1007/BF00497890
19. Phillips, R., Rohani, S. & Baldyga, J. Micromixing in a single-feed semi-batch precipitation process. *AIChE J.* **45**, 82–92 (1999).

20. Hammerschmidt, N., Hobiger, S. & Jungbauer, A. Continuous polyethylene glycol precipitation of recombinant antibodies: Sequential precipitation and resolubilization. *Process Biochem.* (2015). doi:10.1016/j.procbio.2015.11.032
21. Martinez, M., Spitali, M., Norrant, E. L. & Bracewell, D. G. Precipitation as an Enabling Technology for the Intensification of Biopharmaceutical Manufacture. *Trends in Biotechnology* (2019). doi:10.1016/j.tibtech.2018.09.001
22. Hammerschmidt, N., Tscheliessnig, A., Sommer, R., Helk, B. & Jungbauer, A. Economics of recombinant antibody production processes at various scales: Industry-standard compared to continuous precipitation. *Biotechnol. J.* **9**, 766–775 (2014).
23. Zelger, M., Pan, S., Jungbauer, A. & Hahn, R. Real-time monitoring of protein precipitation in a tubular reactor for continuous bioprocessing. *Process Biochem.* **51**, 1610–1621 (2016).
24. Guichardon, P., Falk, L. & Andrieu, M. Experimental Comparison of the Iodide-Iodate and the Diazo Coupling Micromixing Test Reactions in Stirred Reactors. *Chem. Eng. Res. Des.* **79**, 906–914 (2001).
25. Gholap, R. V., Sergio, P. & Bourne, J. R. Influence of viscosity on product distribution of fast competitive chemical reactions. *Chem. Eng. Technol.* **17**, 102–107 (2018).
26. Fournier, M. C., Falk, L. & Villermaux, J. A new parallel competing reaction system for assessing micromixing efficiency - Experimental approach. *Chem. Eng. Sci.* (1996). doi:10.1016/0009-2509(96)00270-9
27. Meakin, M. Y. L. and H. M. L. and D. A. W. and R. K. and R. C. B. and P. Universal diffusion-limited colloid aggregation. *J. Phys. Condens. Matter* **2**, 3093 (1990).
28. Rathore, A. S. & Kateja, N. A coiled flow inversion reactor enables continuous processing. *BioPharm International* (2016).

29. Guichardon, P., Falk, L. & Villermaux, J. Extension of a chemical method for the study of micromixing process in viscous media. *Chem. Eng. Sci.* **52**, 4649–4658 (1997).
30. Hutchinson, N., Bingham, N., Murrell, N., Farid, S. & Hoare, M. Shear stress analysis of mammalian cell suspensions for prediction of industrial centrifugation and its verification. *Biotechnol. Bioeng.* **95**, 483–491 (2006).
31. Chatel, A., Kumpalume, P. & Hoare, M. Ultra scale-down characterization of the impact of conditioning methods for harvested cell broths on clarification by continuous centrifugation-Recovery of domain antibodies from rec E. coli. *Biotechnol. Bioeng.* (2014). doi:10.1002/bit.25164
32. Rousseaux, J. M., Falk, L., Muhr, H. & Plasari, E. Micromixing efficiency of a novel sliding-surface mixing device. *AIChE J.* **45**, 2203–2213 (1999).
33. Yang, K. *et al.* Micromixing Efficiency of Viscous Media in Micro-channel Reactor. *Chinese J. Chem. Eng.* **17**, 546–551 (2009).
34. Gobert, S. R. L., Kuhn, S., Braeken, L. & Thomassen, L. C. J. Characterization of Milli- and Microflow Reactors: Mixing Efficiency and Residence Time Distribution. *Org. Process Res. Dev.* **21**, 531–542 (2017).
35. Panić, S., Loebbecke, S., Tuercke, T., Antes, J. & Bošković, D. Experimental approaches to a better understanding of mixing performance of microfluidic devices. *Chem. Eng. J.* **101**, 409–419 (2004).
36. Gao, Z., Han, J., Bao, Y. & Li, Z. Chinese Journal of Chemical Engineering
Micromixing efficiency in a T-shaped confined impinging jet reactor ☆. **23**, 350–355 (2015).
37. Chan, G., Booth, A. J., Mannweiler, K. & Hoare, M. Ultra scale-down studies of the effect of flow and impact conditions during E. coli cell processing. *Biotechnol. Bioeng.*

(2006). doi:10.1002/bit.21049

38. HOARE, M., DUNNILL, P. & BELL, D. J. Reactor Design for Protein Precipitation and Its Effect on Centrifugal Separation. *Ann. N. Y. Acad. Sci.* (1983). doi:10.1111/j.1749-6632.1983.tb47898.x
39. Boychyn, M., Doyle, W., Bulmer, M., More, J. & Hoare, M. Laboratory scaledown of protein purification processes involving fractional precipitation and centrifugal recovery. *Biotechnol. Bioeng.* **69**, 1–10 (2000).
40. Godawat, R., Konstantinov, K., Rohani, M. & Warikoo, V. End-to-end integrated fully continuous production of recombinant monoclonal antibodies. *J. Biotechnol.* **213**, 13–19 (2015).
41. Kang, Y. K. *et al.* Development of a novel and efficient cell culture flocculation process using a stimulus responsive polymer to streamline antibody purification processes. *Biotechnol. Bioeng.* **110**, 2928–2937 (2013).

Figure Captions

Fig. 1 Schematic illustrations of the continuous tubular reactors employed for mAb precipitation. (A) Lab-scale reactor consists of a double-barrel syringe pump feeding solutions through 0.5 mm diameter tubing into a micro-Tee also of 0.5 mm internal diameter, and finally outlet tubing of a defined diameter and length, arranged in a coil of 16.5 cm diameter. Image of micro-T was obtained by computed tomography. (B) Pilot scale reactor consists of two pumps (main and gradient pump) from an AKTA Ready system, feeding solutions through a stainless steel T of 4.8 mm internal diameter, and finally outlet tubing of 6.4 mm diameter tubing arranged as a coiled-flow inversion reactor around a PVC pipe.

Fig. 2 Determined micro-mixing times, t_m , in the (A) lab-scale and (B) pilot-scale continuous tubular reactors, as a function of Reynolds number Re . Data represent the mean mixing time with ± 1 SD from triplicate experiments.

Fig. 3 Change in the mean particle size of clarified cell culture fluid protein precipitates as a function of flow rate over various reactor lengths in 1 mm diameter tubing. Flow rate represents the total flow rate through the reactor. Ammonium sulphate concentration: 1.5 M, mAb concentration in cell culture fluid: 0.8 mg/mL. All precipitations were carried out at pH 7 and ambient temperature. Data represent the average mean particle size values with ± 1 SD from triplicate experiments.

Fig. 4 Representative micrograph images of protein precipitates obtained at (A) 1 ml/min, (B) 2 ml/min, (C) 4 ml/min, (D) 7 ml/min, (E) 10 ml/min, (F) 14 ml/min. Bar size indicates 20 μ m.

Fig. 5 Effect of protein concentration on the mean particle size at various flow rates with reactor length fixed at 5 m. Data represents the average mean particle size values with ± 1 SD from triplicate experiments.

Fig. 6 (A) Effect of tube diameter on mean precipitate sizes as a function of Re . (B) Energy dissipation correlation with mean particle size.

Fig. 7 (A) Mean precipitate sizes in the pilot-scale continuous tubular reactor from duplicate runs. (B) Representative PSD profiles for (i) 9 L/H, (ii) 20 L/H, (iii) 90 L/H and (iv) 150 L/H. (C) Energy dissipation vs. mean particle size for lab-scale and pilot-scale reactors.

Fig. 8 Effect of turbulent processing in a rotating disc device on lab-scale protein precipitates formed from various flow rate conditions. Tube diameter: 1 mm. Experiments were performed in triplicate.

Fig. 9 Effect of turbulent processing in a rotating disc device on pilot-scale protein precipitates formed from various flow rate conditions. Data are presented from two sets of runs.

Fig. 10 Ultra-scale down centrifugation analysis of non-sheared (black squares) and sheared (red circles) lab-scale precipitate samples. Centrifugal efficiency is characterised in terms of percentage of solids remaining, S , in the supernatant as a function of centrifuge throughput. Precipitates were prepared at (A) 1 ml/min, (B) 2 ml/min, (C) 4 ml/min, (D) 7 ml/min, (E) 10 ml/min, (F) 14 ml/min and (G) 20 ml/min in the lab-scale reactor with 1 mm diameter tubing. Data are presented as averages of $n = 4 \pm 1$ standard deviation and fitted with linear regression.

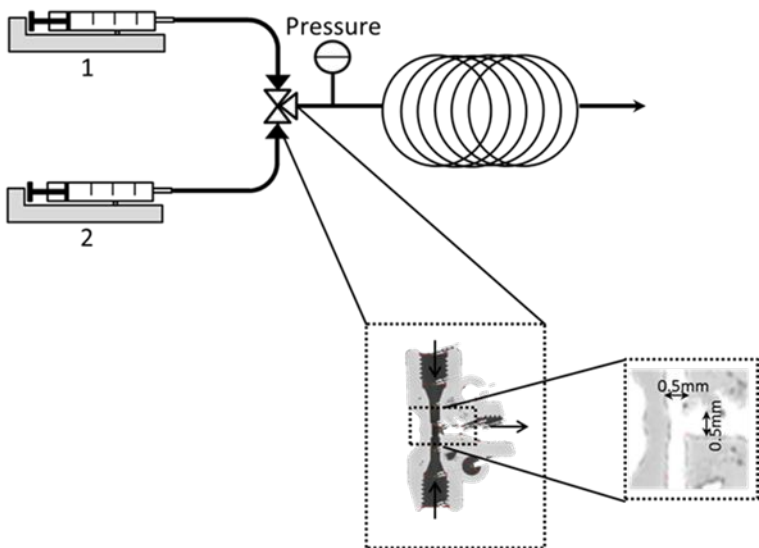
Fig. 11 Ultra-scale down centrifugation analysis of non-sheared (black squares) and sheared (red circles) pilot-scale precipitate samples. Centrifugal efficiency is characterised in terms of percentage of solids remaining, S , in the supernatant as a function of centrifuge throughput. Precipitates were prepared at (A) 9 L/H, (B) 20 L/H, (C) 90 L/H and (D) 150 L/H. Data are presented as averages of $n = 4 \pm 1$ standard deviation and fitted with linear regression.

Fig. 12 (A) PSD profiles of precipitate feed, centrate and discharged solids during processing on Pathfinder PSC-1 centrifuge. Each profile corresponds to the technical average measurement of $n = 5$ particle size measurements and is shown in terms of volume percentage. (B) Representative micrograph of precipitate feed from the pilot-scale reactor

operating at 150 L/H. (C) Representative micrograph of precipitate solids discharged from centrifuge bowl. Disc-stack centrifugation was performed at 13000 x g and 35 L/H.

Figure 1

(A)



(B)

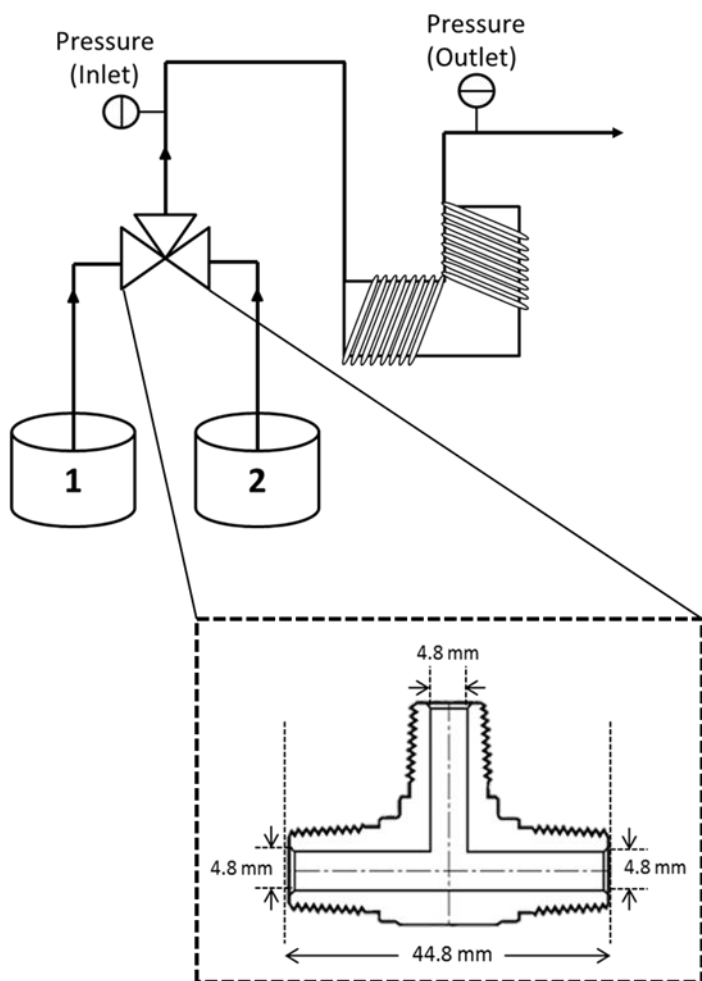
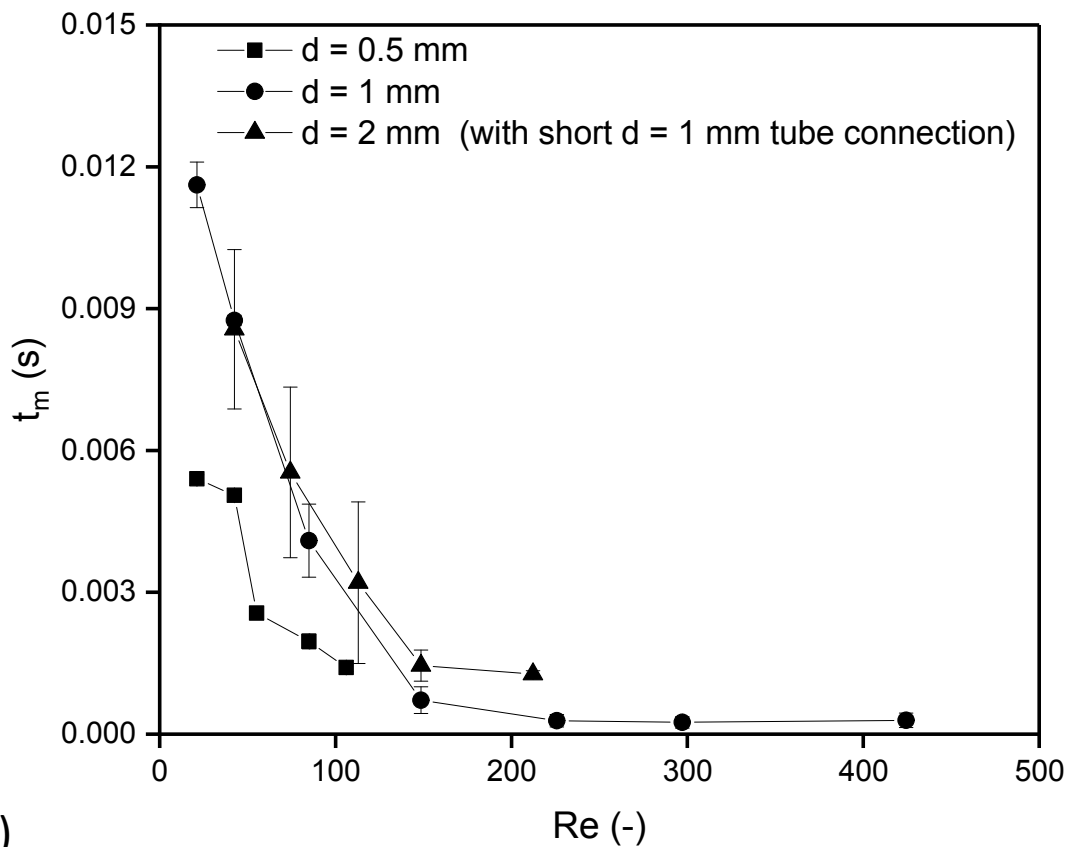


Figure 2

(A)



(B)

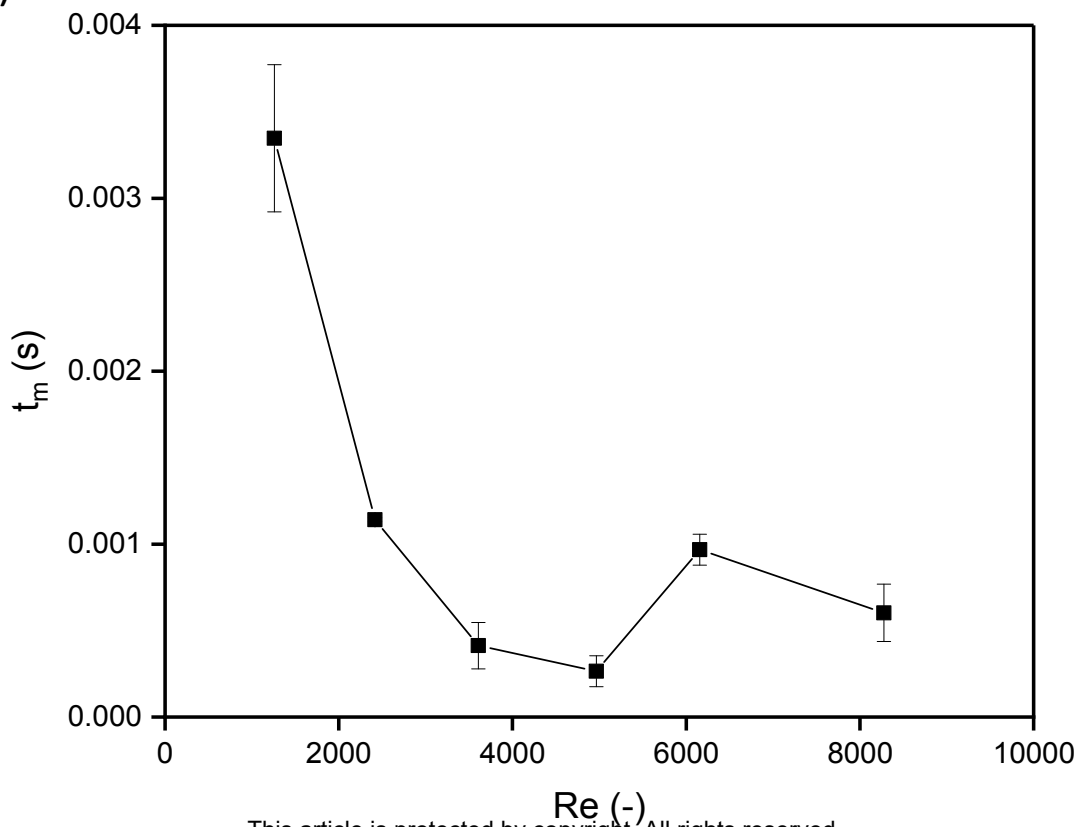


Figure 3

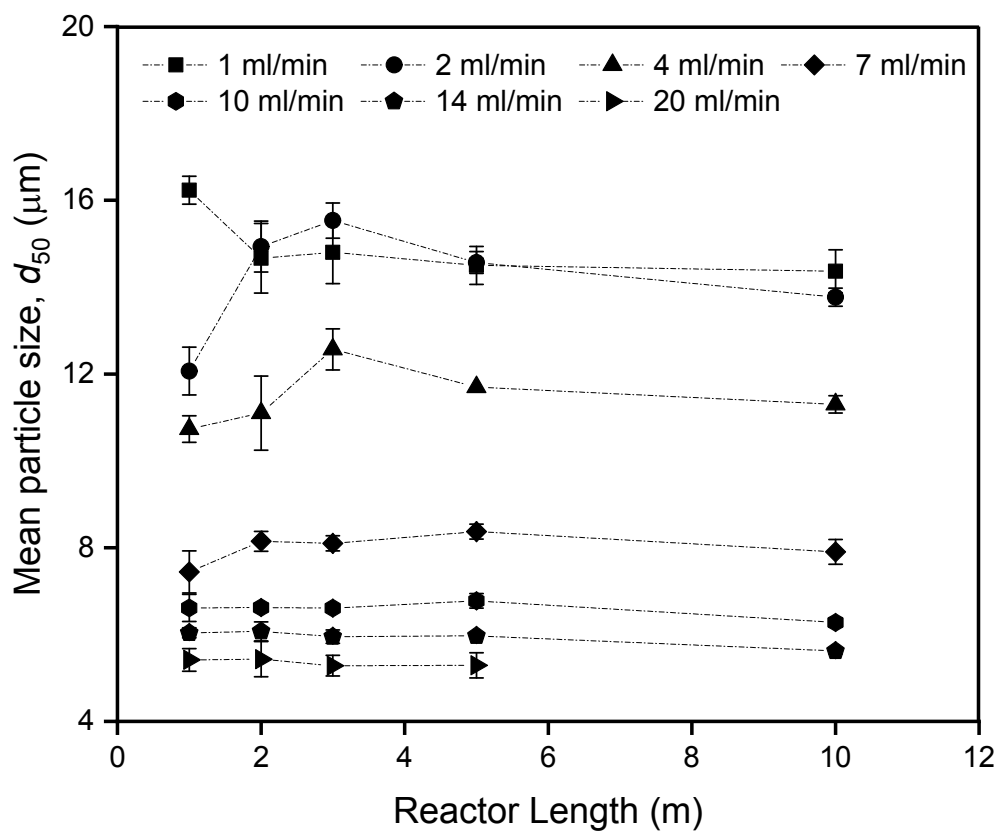


Figure 4

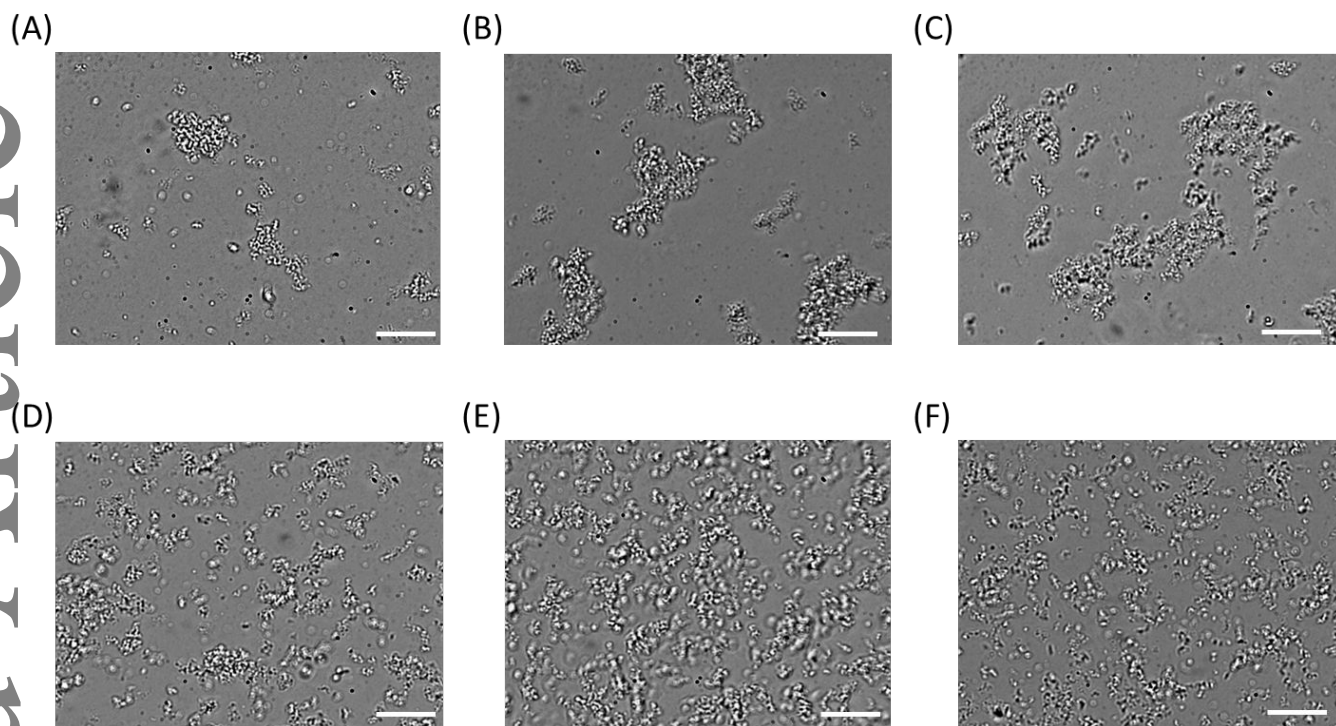


Figure 5

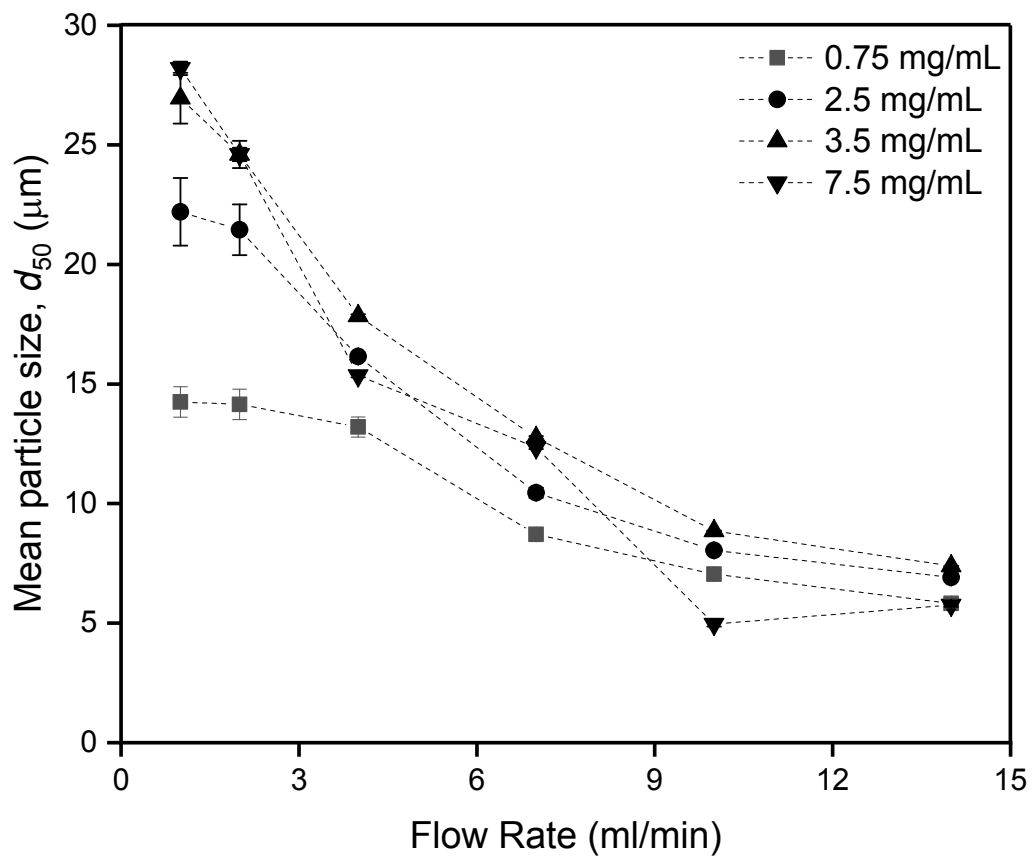


Figure 6

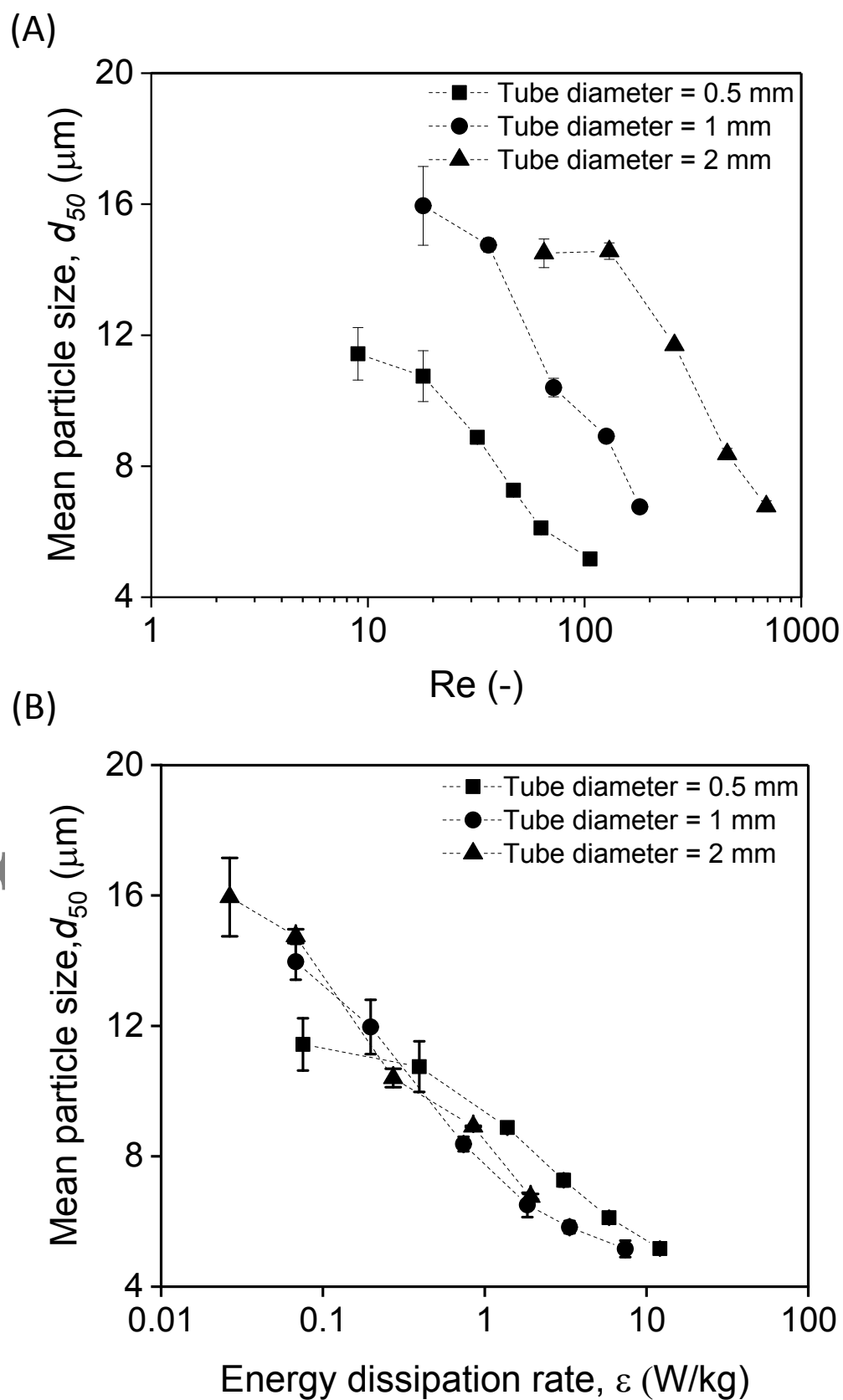


Figure 7

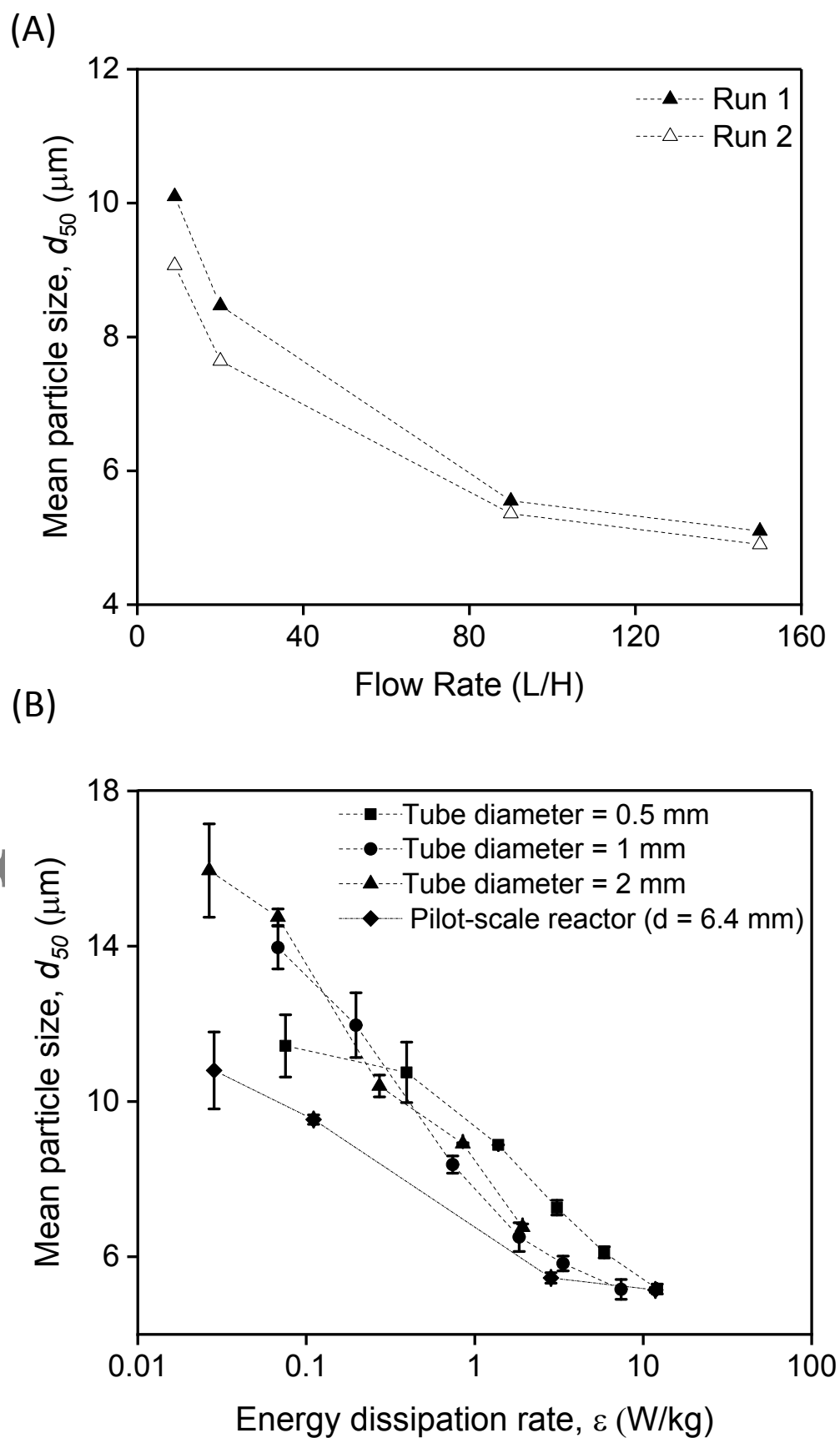


Figure 8


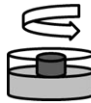
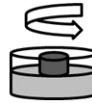
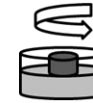


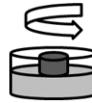
Flow Rate (ml/min)	1	2	4	7	10	14	20
Reactor Shear Rate (s^{-1})	116	240	480	850	1248	1648	2502
Mean Particle Size d_{50} (μm) \pm Std. Deviation	14.7 ± 0.55	14 ± 0.6	11.9 ± 0.83	8.37 ± 0.22	6.51 ± 0.37	5.83 ± 0.2	5.2 ± 0.25
Fractal Dimension, f_D (-) \pm Std. Deviation	2.27 ± 0.01	2.31 ± 0.01	2.42 ± 0.02	2.53 ± 0.01	2.74 ± 0.05	2.84 ± 0.02	2.87 ± 0.02
Rotary Disc Shear Device (Shear Rate = $100 s^{-1}$)							
Mean Particle Size d_{50} (μm) \pm Std. Deviation	5.88 ± 0.52	5.45 ± 0.85	6.44 ± 1.2	4.73 ± 0.33	4.29 ± 0.15	4.32 ± 0.3	4.17 ± 0.42
Percentage Size Reduction (%)	60	56	46	44	34	26	20

Figure 9

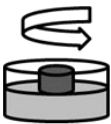
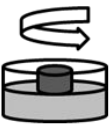
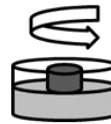
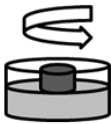
Flow Rate (L/H)		9	20	90	150
Reactor Shear Rate (s^{-1})		155	306	1550	3165
Mean Particle Size d_{50} (μm)	<i>Run 1</i>	10.1	9.45	5.36	5.1
	<i>Run 2</i>	11.5	9.62	5.55	5.19
Fractal Dimension, f_D (-)	<i>Run 1</i>	2.31	2.37	2.73	2.86
	<i>Run 2</i>	2.35	2.42	2.72	2.83
Rotary Disc Shear Device (Shear Rate = $100 s^{-1}$)					
Mean Particle Size d_{50} (μm)	<i>Run 1</i>	4.3	4.2	4.25	4.55
	<i>Run 2</i>	4.8	4.38	4.83	4.33
Percentage Size Reduction (%)	<i>Run 1</i>	57	55	21	11
	<i>Run 2</i>	58	54	13	17

Figure 10

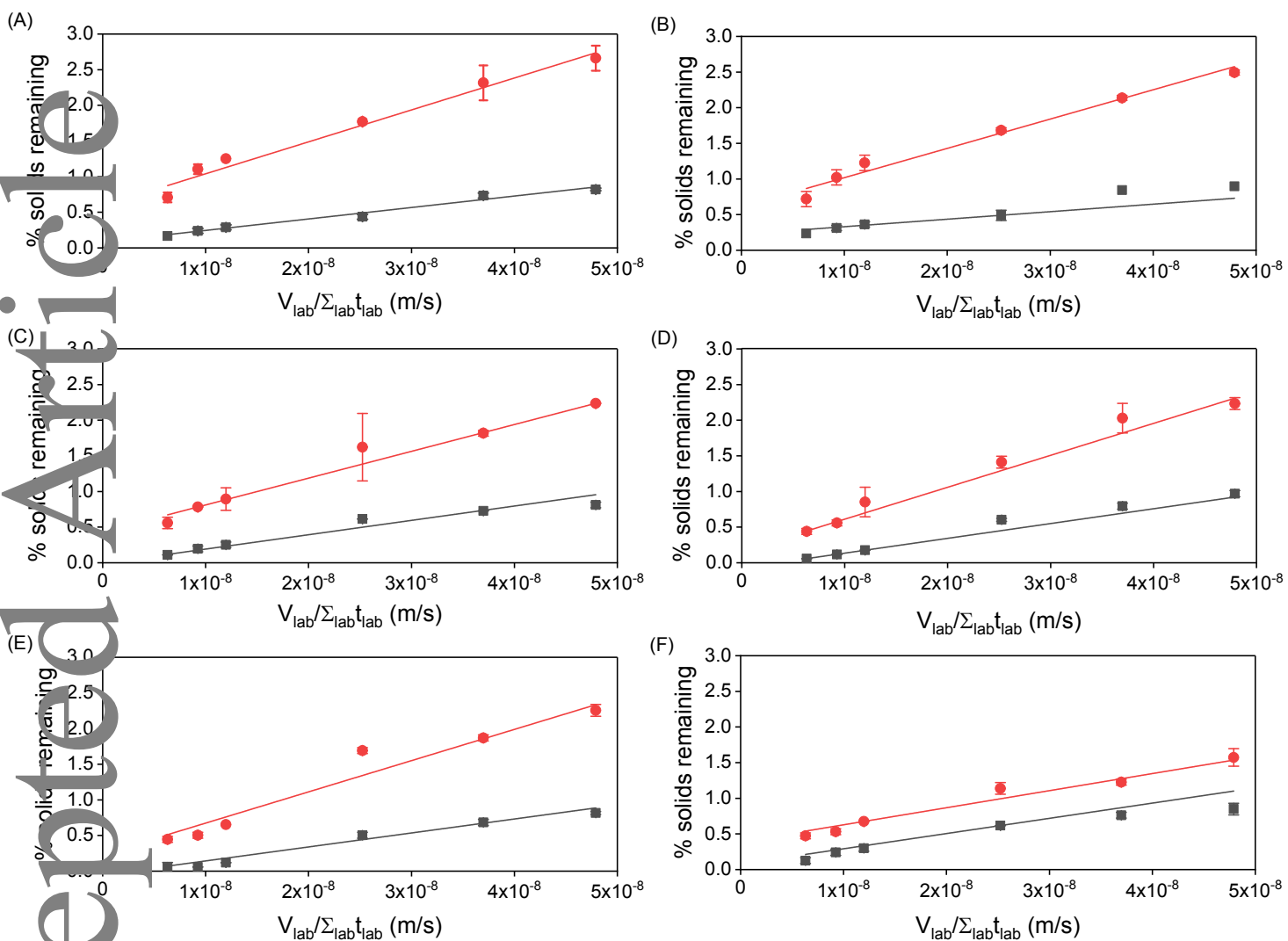


Figure 11

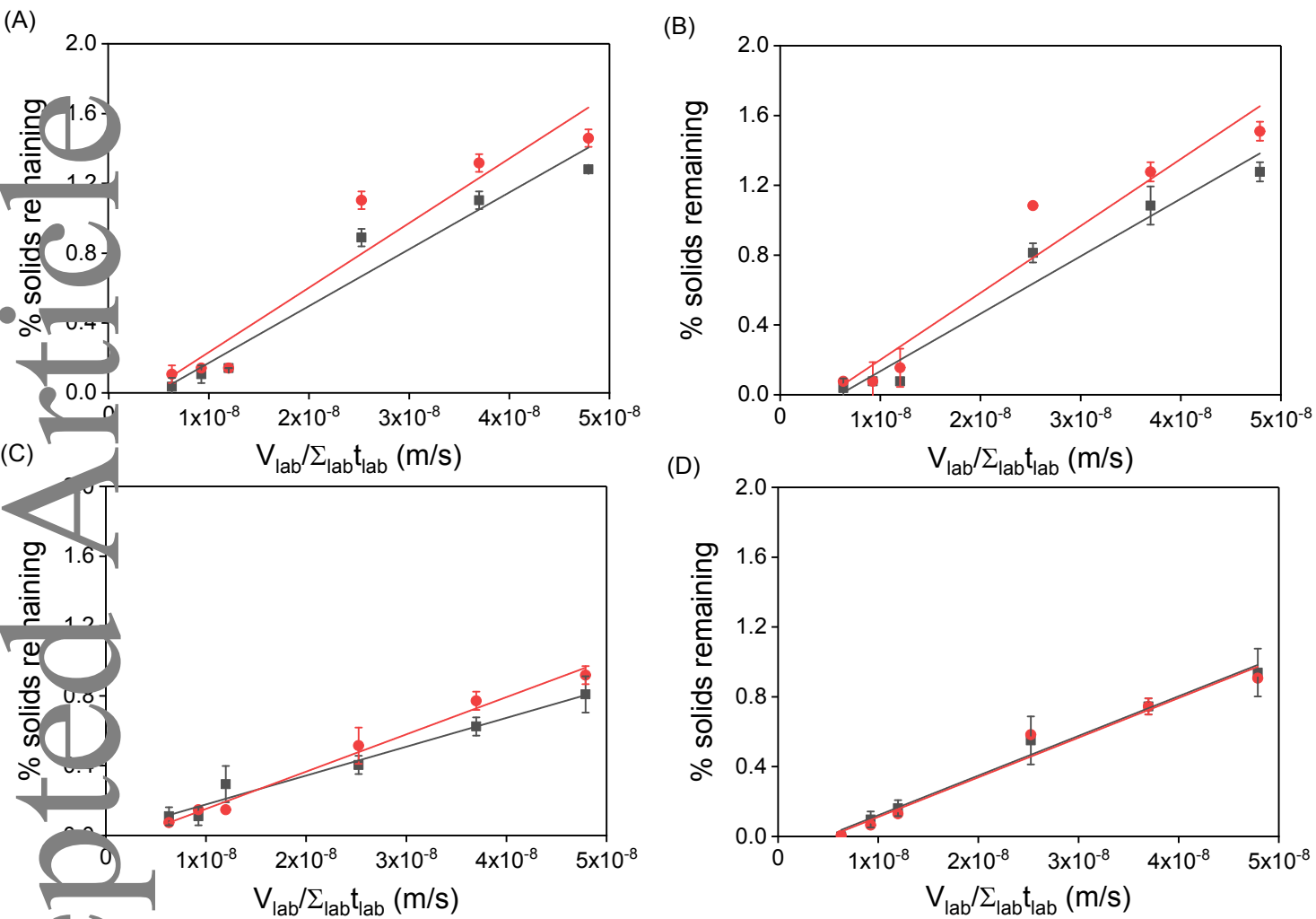


Figure 12

